NASA TN D-777

TECHNICAL NOTE

D-777

BALLISTIC RANGE MEASUREMENTS OF STAGNATION-POINT HEAT TRANSFER IN AIR AND IN CARBON DIOXIDE AT VELOCITIES UP TO 18,000 FEET PER SECOND

By Layton Yee, Harry E. Bailey, and Henry T. Woodward

Ames Research Center
Moffett Field, Calif.

NATIONAL AERONAUTICS AND SPACE ADMINISTRATION

WASHINGTON March 1961

1T

NATIONAL AERONAUTICS AND SPACE ADMINISTRATION

TECHNICAL NOTE D-777

BALLISTIC RANGE MEASUREMENTS OF STAGNATION-POINT HEAT TRANSFER IN AIR AND IN CARBON DIOXIDE AT VELOCITIES UP TO 18,000 FEET PER SECOND

By Layton Yee, Harry E. Bailey, and
Henry T. Woodward

SUMMARY

A new technique for measuring heat-transfer rates on free-flight models in a ballistic range is described in this report. The accuracy of the heat-transfer rates measured in this way is shown to be comparable with the accuracy obtained in shock-tube measurements. The specific results of the present experiments consist of measurements of the stagnation-point heat-transfer rates experienced by a spherical-nosed model during flight through air and through carbon dioxide at velocities up to 18,000 feet per second. For flight through air these measured heat-transfer rates agree well with both the theoretically predicted rates and the rates measured in shock tubes. For flight through carbon dioxide the heat-transfer rates agree well with the rates measured in a shock tube. Two methods of estimating the stagnation-point heat-transfer rates in carbon dioxide are compared with the experimental measurements. At each velocity the measured stagnation-point heat-transfer rate in carbon dioxide is about the same as the measured heat-transfer rate in air.

INTRODUCTION

The purpose of this report is twofold. A method of measuring heat-transfer rates in a ballistic range is described, and results are presented which were obtained by this method for the stagnation-point heat-transfer rate encountered by a spherical-nosed body flying through air and through carbon dioxide. The choice of carbon dioxide has been prompted by its predicted presence in the atmosphere of Venus.

Most of the experimental results on heat-transfer rates through highly cooled boundary layers have been obtained from measurements made in shock tubes. The shock tube correctly simulates the stagnation enthalpy which is the parameter of major interest in heat-transfer measurements. Unfortunately, the shock tube, as it is ordinarily used, does not correctly

mulate either the Mach number or the Reynolds number. The ballistic nge technique correctly simulates both the Mach number and the stagnaon enthalpy. Of course, the actual size of the model is not correctly produced in either the range or the shock tube; however, in the range is possible to vary the Mach number and Reynolds number independently that nonequilibrium effects due to the small size of the model can studied.

All the measurements of stagnation-point heating rates presented in is report have been made at an ambient temperature of 540° R and an bient pressure of 1/10 of an atmosphere. For these conditions the stagtion density is sufficiently high, approximately atmospheric, that the ow in the shock layer is in thermal and chemical equilibrium in spite the small size of the model.

The authors would like to acknowledge the assistance of . W. J. Kerwin in the design of the thermocouple model and the coils ed to pick up the signals transmitted by the model. Interpretation of e signal picked up by the coils required an analysis of the variation coil response with the dispersion in flight path from the coil's exact ıter. The authors wish to acknowledge the contribution of W. A. Mersman in carrying out this analysis and the resulting putations.

SYMBOLS

radius of pickup coil

radius of model coil

ballistic coefficient

length of pickup coil

specific heat at constant pressure

drag coefficient

distance between coil centers

internal energy

emf induced in pickup coil

free-energy change

constant in least squares straight line, defined in equation (4)

slope of least squares straight line, defined in equation (5)

h	enthalpy
I	current in model coil
K_p	equilibrium constant for constant pressure
k	thermal conductivity
L	Lewis number
l	thickness of copper nose cap
M	mutual inductance
m	molecular weight
m_p	mass of the model
N	number of turns in coil
Nu	Nusselt number
n	index of summation
P	pressure
$\dot{q}$	stagnation-point heat-transfer rate
R	universal gas constant
Re	Reynolds number
S	cross-sectional area of model
T	temperature
t	time
U_e	flow velocity at outer edge of boundary layer behind shock wave, βy
V	flight velocity of model
X	mole fraction
x	distance into copper cap
y	distance along copper cap measured from stagnation point
Z	compressibility
z	distance along model trajectory

α	diffusivity of copper
β	velocity gradient measured along the copper cap at stagnation point
μ	viscosity
ν	kinematic viscosity
ρ	density
τ	dummy variable

Subscripts

A	pickup coil
a	model coil
Cu	copper cap
D	dissociation
e	external flow
i	component of gas mixture
o	conditions at $z = 0$ and $t = 0$
P	constant pressure
s	stagnation point
std	standard conditions
t	differentiation with respect to time
w	fluid properties at wall
x	differentiation with respect to distance into copper cap
I	chemical reaction, dissociation of carbon dioxide
II	chemical reaction, dissociation of oxygen
1	conditions ahead of shock wave
2	conditions behind shock wave

EXPERIMENTAL PROCEDURE

Description of Apparatus

All the heat-transfer rates reported herein have been made on small models in free flight. The models were launched from a light-gas gun of the type described in reference 1. The ballistic range is instrumented with spark shadowgraphs and electronic chronographs, as well as the pickup coils described in a subsequent paragraph.

The construction of the model is shown in figure 1. The model consisted of a hemispherical nose with a short cylindrical section and a 120° conical tail. The body of the model was made of 2024-T4 aluminum, chosen for its high strength-to-weight ratio. The model was held in a four-piece nylon sabot during launch.

A 0.0075-inch-thick copper cap on the nose of the model acted as a calorimeter heat gage. A constantan wire, silver soldered to the cap at the stagnation point of the model, formed the hot junction of a copper-constantan thermocouple. This constantan wire, kept small (0.006-inch diameter) near the nose of the model to minimize the conduction of heat away from the stagnation point, enlarged to 0.025-inch diameter and extended back to the center of the model to form the cold junction of the thermocouple with a copper disc. A four-turn coil wound on a boron nitride form was connected between the two junctions of the thermocouple at the disc in the center of the model and at a point on the periphery of the nose cap. Cement was used to join all mating surfaces. To permit computation of temperature rise, the electrical resistance of the complete circuit was accurately measured before final assembly.

The pickup coil was made of B and S gage No. 40 Formvar coated copper magnet wire, wound on a Fiberglas form. The coil was a 1-layer, 400 turn, center-tapped coil, 4 inches in diameter and 1-1/2 inches long. Electrostatic shielding was incorporated in the coil form to eliminate spurious signals resulting from the static charge of the model, the wake, and the propellant gases. The inside shielding consisted of B and S gage No. 24 soft copper wires imbedded in the coil form, spaced 1/8 inch apart and parallel to the axis of the coil. The shielding wires were 1/32 inch from the inside diameter of the coil form. Every other wire was cut off at one end of the coil form and connected at the opposite end to a B and S gage No. 12 copper wire, which was in the shape of an open-ended copper ring, so that there were no shorted turns in the shielding. The elimination of shorted turns prevented the model magnetic field from inducing a current in the shield which might distort the emf induced in the pickup coil. The shielding was completed outside the coil by B and S gage No. 24 soft copper wires, spaced 1/4 inch apart and parallel to the axis of the coil. Thus, the entire coil was in an electrostatic Faraday cage. The construction of the coil is shown in figure 2.

As the stagnation point is heated during the flight of the model, the resulting potential difference between the hot junction and the cold junction causes a current to flow in the model coil, thus producing a magnetic field around the model. This magnetic field in turn induces an emf on the pickup coils located along the trajectory of the model. There are six pickup coil stations, the first of which is approximately nine feet from the muzzle and the last approximately 34 feet from the muzzle. Each coil station, located about 3 feet down range of a shadowgraph station, consists of a pickup coil connected to a Tektronix type 535 oscilloscope with a type D high-gain differential input plug-in preamplifier. As the model flies down the range, it interrupts a photobeam which triggers the spark gap in the shadowgraph station. When the spark gap fires, it simultaneously gives a shadowgraph of the model and triggers the sweep of the recording oscilloscope which is connected to the pickup coil. The experimental setup is shown schematically in figure 3. The magnitude of the voltage induced on a pickup coil is a function of the velocity and position of the model with respect to the pickup coil, as well as the temperature difference of the thermocouple. Therefore, if the velocity and position of the model are known, the temperature difference of the thermocouple in the model can be computed from the oscilloscope record. Even though the model coil is contained in a metal body and surrounded in flight by an ionized layer of gas, no difficulty in transmitting the signal to the pickup coil is experienced. This is because the current flowing in the model coil varies slowly over the length of the range, so that the frequency of the signal is effectively direct current, and the counter electromotiveforces from the currents induced in the body shell and the ionized layer are negligible.

A 4 2 7

Appendix A contains the details of the computation of the temperature history of the copper cap from the oscilloscope records in terms of the electrical parameters of the system. It should be mentioned at this point that the effective temperature of the hot junction of the thermocouple will be the lowest temperature present at the junction, since any currents induced by temperature differences at the hot junction are short circuited and, hence, produce no net flow through the circuit. In the present case, since the constantan stem extended through the copper cap, this lowest temperature will be the temperature of the inside or rear surface of the copper cap. A typical oscilloscope record is shown in figure 4. The disturbances on either side of the signal are caused by the spark discharges of the shadowgraph stations.

Data Reduction

As indicated in the preceding section, the raw experimental results consist of the temperature history of the inside or rear surface of the copper cap calorimeter. In order to present the data in the most usable form, it is necessary to compute the heat-transfer rate at the stagnation

point from this temperature history. Toward this end the following assumptions are made:

(a) The heat flow is one-dimensional.

(b) None of the heat transferred to the model penetrates beyond the inner surface of the copper cap.

(c) No temperature gradient exists between the front and the rear surfaces of the copper cap.

The heat-transfer rate is then given by,

$$\dot{q} = \frac{k_{Cu} l}{\alpha} \frac{dT}{dt} \qquad (1$$

where α is the diffusivity of copper, k_{Cu} is the thermal conductivity of copper, and l is the thickness of the copper cap. Assumption (a) i satisfied since the heat-transfer rate does not vary by more than 5 perc over the entire front surface of the copper cap, and assumption (b) is v well fulfilled since the boron nitride behind the copper cap is a good h insulator. Assumption (c) is intimately related to the finite response time of the copper cap calorimeter gage. It is shown in appendix B that the error incurred in making assumption (c) is less than 2 percent for the present experiments.

Since there is a certain amount of experimental error in the temperatures measured at the various pickup coil stations, the problem of fitting the proper temperature history function to the data points must be considered. For small changes in the velocity the heat-transfer rate may be assumed proportional to the cube of the velocity,

$$\dot{q} = \dot{q}_o \left(\frac{V}{V_o}\right)^3 \qquad (2$$

For flight at sufficiently high Mach numbers the drag coefficient is approximately constant, so that

$$\frac{dV}{dt} = -BV^2 \qquad (3$$

where $B = (\rho C_D S)/(2m_p)$ is the ballistic coefficient for the model. The ballistic coefficient may be determined for each round from a plot of $1/V$ versus t, as indicated in reference 2. Equations (1), (2), and (3) may be combined to give,

$$T = f + g\left(\frac{V}{V_o}\right)^2 \qquad (4)$$

where

$$g = -\frac{\alpha \dot{q}_o}{2k_{Cu} l B V_o} \qquad (5)$$

For each round the temperature is plotted against the square of the velocity, and the straight line giving the best least squares fit is found. The slope of this line together with the ballistic coefficient, the copper cap thickness, and the thermal properties of copper then determine the heat-transfer rate $\dot{q}_o$. The thermal conductivity and the thermal diffusivity of copper were taken from reference 3.

The procedure outlined above yields a value of $\dot{q}_o$ corresponding to the value of the muzzle velocity, V_o, for each round fired. Equation (2) then gives the value of $\dot{q}$ which corresponds to a given value of V, where V is less than the muzzle velocity, V_o, but greater than the velocity at the last pickup coil. The heating rate $\dot{q}_o$ is a function of the velocity of the model and the temperature of the outer surface of the copper cap. Both of these quantities change along the trajectory of the model. For example, at high muzzle velocities the heating rates will be higher, and thus the surface temperature will be higher at each pickup coil than it would be for a low muzzle velocity. However, in analyzing the data it is desirable to eliminate the surface temperature as a variable. Therefore, a specific value of the surface temperature is selected, and from each round the values of $\dot{q}$ and V which correspond to the selected surface temperature are determined as follows: The difference in temperature between the inner and outer surfaces of the copper cap calorimeter is estimated using the graphical technique of Schmidt (see ref. 4) and the value of $\dot{q}_o$ appropriate to the particular round under consideration. This temperature difference is then subtracted from the specified value of the outer surface wall temperature to give the temperature on the inner surface of the copper cap. The velocity which corresponds to this temperature is then found from the plot of temperature versus the square of the velocity mentioned in the preceding paragraph. The proper value of $\dot{q}$ can then be computed from equation (2). Thus each round fired gives one value of $\dot{q}$ at the specified wall temperature and a particular velocity. For the present series of experiments a wall temperature of 900° R was selected since this temperature occurred before the last pickup coil on the low velocity rounds and after the first pickup coil on the high velocity rounds.

DISCUSSION OF RESULTS

Heating in Air

The main purpose of the present experiments was to measure stagnation-point heat-transfer rates in carbon dioxide. However, in order to compare the results obtained by the present measuring technique with the extensive shock tube measurements, several rounds were fired in air at a pressure of 76-mm Hg and a temperature of 540° R. The measured heat-transfer rates are plotted versus velocity in figure 5. The rates predicted by the theory of reference 5 are shown as the solid line, and those predicted by the theory of reference 6 are shown as the dashed line.

In addition, some of the results of the shock tube measurements reported in reference 7, corrected to the present test conditions by the method outlined in reference 10, are shown in figure 5. The agreement of the present measurements with the theory of reference 5 and the shock-tube measurements is good. The rates given by the theory of reference 6 are lower than the measured values.

The heat-transfer rates are replotted in dimensionless form in figure 6. The heat-transfer parameter is the Nusselt number divided by the square root of the Reynolds number. These dimensionless parameters are defined by

$$Nu = \frac{\dot{q}_y c_{p_w}}{k_w(h_s - h_w)} \tag{6a}$$

$$Re = \frac{U_e y}{\nu_w} = \frac{\beta y^2}{\nu_w} \tag{6b}$$

The heat-transfer parameter is then

$$\frac{Nu}{\sqrt{Re}} = \frac{\dot{q} c_{p_w}}{k_w(h_s - h_w)} \sqrt{\frac{\nu_w}{\beta}} \tag{7}$$

The properties of air necessary for the evaluation of these parameters were taken from references 8 and 9. The viscosity was obtained from Sutherland's formula. The velocity gradient at the stagnation point, β, was computed from the Newtonian approximation given in reference 5. It is apparent from figure 6 that the present experimental results agree very well with the theory of reference 5. Again it is clear that the heat-transfer rates predicted by the theory of reference 6 are low.

Heating in Carbon Dioxide

Most of the heat-transfer measurements were made in carbon dioxide at a pressure of 76-mm Hg and a temperature of 540° R. There was a maximum of 5 percent air in the test gas because of unavoidable leaks in the flight-test chamber. Although the effect of the air on heat-transfer rate is unknown, it is very likely quite small for the conditions of the present tests.

The measured heat-transfer rates are plotted versus velocity in figure 7. In addition, the experimental results of reference 10, which were obtained in a shock tube using a mixture of 90 percent carbon dioxide and 10 percent nitrogen, are shown for comparison. These shock tube results have been corrected to the ambient conditions of the range measurements.

No theoretical analysis such as that of reference 5 has been made for the case of carbon dioxide. The analysis of reference 5 implicitly contains the real gas properties of air in the variation of $\rho\mu$ through the boundary layer. Since the heat transfer is not sensitive to the details of this variation, it is proposed here to use the equations for the heat-transfer rate obtained in reference 5 for air, but to substitute the thermodynamic and transport properties of carbon dioxide for those of air wherever they occur in the final formulas. Although these formulas call for the use of properties at the stagnation point, the properties just behind the shock wave are used since the difference in the final result is negligible. The thermodynamic properties of carbon dioxide at the temperatures and pressures encountered behind a normal shock wave at velocities up to 20,000 feet per second have been computed as outlined in appendix C. The viscosity of carbon dioxide was evaluated from Sutherland's formula with $C = 432^{\circ}$ R. The properties of carbon dioxide at the wall temperature were obtained from reference 9.

A second method of predicting the theoretical heat-transfer rate is given in reference 6. The dashed curve in figure 7 shows the heat-transfer rate predicted by this theory. In order to compute the heat-transfer rate according to this theory, it is necessary to obtain the integral with respect to temperature of the thermal conductivity of carbon dioxide from the wall temperature to the stagnation temperature. These data were obtained from the results of reference 11.

When compared with the theory of reference 5, the present measurements give a standard deviation of ±11 percent. The standard deviation for the shock-tube measurements for comparison with the same theory is ±12 percent. Hence, it may be inferred that the accuracy of measurement is substantially the same for both systems.

The heat-transfer rates in carbon dioxide are replotted in dimensionless form in figure 8. The dimensionless parameters have been determined from equations (6) and (7). The stagnation-point velocity gradient has been computed from the Newtonian approximation of reference 5.

The theory of reference 6 gives a better estimate than the theory of reference 5 for the heating rate in carbon dioxide for Mach numbers from 12 to 20. However, neither theory satisfactorily predicts the variation of heating rate with Mach number. Both theories indicate a decrease in heat-transfer parameter with an increase in Mach number, whereas the experimental results indicate practically no variation of heat-transfer parameter with Mach number; consequently, caution should be exercised in using either theory at Mach numbers above 20.

The effect on the heat-transfer rate of changing the gas from air to carbon dioxide may be seen by comparing figures 5 and 7 or figures 6 and 8. The ambient pressures and temperatures are the same in both cases. The important result is that the heat-transfer rates measured in carbon dioxide are of the same magnitude as those measured in air.

CONCLUSIONS

A novel method of measuring heat-transfer rates in a ballistic range has been developed. The accuracies attainable with this method compare favorably with the accuracies attainable in shock-tube measurements of heat-transfer rates.

The potentiality of the system described herein lies in two directions. Mach number and Reynolds number can be varied independently and heat-transfer measurements can be made near the base of the model without fear of interference from a supporting structure.

The measured values of stagnation-point heat-transfer rates in air agree well with the theory of reference 5, but are higher than the rates predicted by the theory of reference 6. The measured values of stagnation-point heat-transfer rates in carbon dioxide agree fairly well with the theory of reference 6, but lie below the values predicted by the theory of reference 5. Neither theory, however, correctly predicts the nearly constant value of heat-transfer parameter, $Nu/\sqrt{Re}$, with change in Mach number which is shown by the experimental measurements. The measured values of heat-transfer rate in carbon dioxide are approximately the same as those measured in air.

Ames Research Center
National Aeronautics and Space Administration
Moffett Field, Calif., Jan. 11, 1961

APPENDIX A

TEMPERATURE HISTORY OF COPPER CAP CALORIMETER GAGE FROM COIL RESPONSE

When the model is in flight and the stagnation point is heated, the temperature rises at the hot junction of the thermocouple in the copper calorimeter cap. The cold junction at the other end of the constantan rod inside the model far from sources of heat remains effectively at the ambient temperature of the model prior to launch during the very short time of flight through the range. This temperature difference of the hot and cold junctions of the thermocouple results in an emf, causing a current to flow in the model coil. The current flow produces a magnetic field which induces an emf in the pickup coil as the model passes through it.

A 4 2 7

The voltage induced in the pickup coil by the moving model is given by Faraday's law

$$e = - \frac{d(MI)}{dt} \tag{A1}$$

where

e emf induced in pickup coil

M mutual inductance between the two coils

I current flowing in the model coil

If it is assumed that the current in the model coil is constant during the short time that it takes the model to pass through the pickup coil, the voltage induced in the pickup coil is

$$e = -I \frac{dM}{dt} \tag{A2}$$

From reference 12, the mutual inductance between the two coils may be expressed as:

$$M = 0.0250 \frac{a^2 N_a N_A}{b} \left[\frac{D + b}{\sqrt{(D + b)^2 + A^2}} - \frac{D - b}{\sqrt{(D - b)^2 + A^2}} \right] \tag{A3}$$

where

a radius of smaller coil, in.

A radius of larger coil, in.

$2b$ length of the larger coil, in.

N_a total number of turns on the smaller coil

N_A total number of turns on the larger coil

D axial distance between the centers of the coils, in.

M mutual inductance in microhenries

Substituting the appropriate values and expressing the mutual inductance in terms of the distance between coils yields the equation

$$M = 0.342\left[\frac{D + 0.75}{\sqrt{(D + 0.75)^2 + 4}} - \frac{D - 0.75}{\sqrt{(D - 0.75)^2 + 4}}\right] \tag{A4}$$

Since $dM/dt = V(dM/dD)$, differentiation of equation (A4) with respect to time followed by substitution into equation (A2) gives

$$e = -1.368\times10^{-6}IV\left\{\frac{1}{[(D + 0.75)^2 + 4]^{3/2}} - \frac{1}{[(D - 0.75)^2 + 4]^{3/2}}\right\} \tag{A5}$$

Because it is more convenient to reduce the data by using the peak voltage recorded on the oscilloscope, the above equation is differentiated to find the value of D for which e is a maximum. When this value of D is substituted in (A5),

$$e_{max} = -0.096\times10^{-6}IV \tag{A6}$$

where V is the velocity of the model in inches per second when the model is halfway through the pickup coil, I is in amperes, and e_{max} is in volts. Equation (A6) is valid for those cases in which the frequency response of the pickup coil and oscilloscope is flat. The flat portion of the frequency response can, of course, be extended by properly damping the combination of pickup coil inductance and oscilloscope capacitance. Although this was not done for the present tests, it would be necessary at higher velocities. Preliminary calculations indicate that errors from this source will be less than 10 percent for the present measurements.

The peak induced voltage may be measured from the oscilloscope record. The model velocity may be computed from the shadowgraph records and the chronograph readings. Then the current flowing in the model coil may be obtained from equation (A6). The product of the calculated current and the measured model circuit resistance gives the emf output of the

thermocouple. The temperature rise of the copper cap calorimeter may be obtained from the thermocouple calibration curve (fig. 9) after the necessary correction is made for the cold junction at room temperature.

The calculations discussed above are valid for on-center shots only. Since the launching of a model through the exact center of a coil is but a fortuitous occurrence, corrections must be made for off-center shots. For off-center shots the voltage induced in the pickup coil is still given by equation (A2), however the mutual inductance between the two coils is no longer given by equation (A3). A more complicated expression which involves the lateral distance between the axes of the two coils is obtained. This expression has been evaluated on an IBM 650 digital computer.

The correction factor was then experimentally verified by mutual induction measurements as shown by the plotted points in figure 10. The correction factor is applied as a reduction in the measured signal strength to give the effective signal strength which would have been recorded if the model had passed through the coil's center; that is

$$e_{\text{on-center}} = (\text{correction factor})\, e_{\text{off-center}} \qquad \text{(A7)}$$

when $e_{\text{off-center}}$ is the measured value of e and $e_{\text{on-center}}$ is the value to be used in equation (A6).

The magnitude of the signal is also affected by the angle of attack of the model. However, the angle of attack usually is slight or even undiscernible and is considered to be zero for all the data reported herein.

APPENDIX B

TRANSIENT RESPONSE OF CALORIMETER GAGE

The relationship between the temperature history on the rear face of the copper cap and the heat flux into the front face may be determined by solving the following boundary-value problem:

$$\left.\begin{aligned} T_t(x,t) &= \alpha T_{xx}(x,t) \\ T_x(l,t) &= 0 \\ T(x,0) &= 0 \\ -k_{Cu}T_x(0,t) &= \frac{\dot{q}_o}{(BV_o t + 1)^3} \end{aligned}\right\} \tag{B1}$$

where $T(x,t)$ is the temperature at any point x and at any time t, α is the diffusivity, k_{Cu} is the coefficient of heat conduction, $\dot{q}_o$ is the heat flux at time $t = 0$, V_o is the velocity at time $t = 0$, and B is the ballistic coefficient.

A relationship between $T_t(l,t)$ and $\dot{q}_o$ may be found by solving the above problem with the Laplace transform method (ref. 13).

$$T_t(l,t) = \frac{\alpha}{k_{Cu} l}\left(\frac{\dot{q}_o}{(BV_o t + 1)^3} + 2\sum_{n=1}^{\infty}(-1)^n\left\{\int_o^t \frac{-3BV_o\dot{q}_o}{[BV_o(t-\tau)+1]^4} e^{-\frac{n^2\pi^2\alpha\tau}{l^2}}\right.\right.$$

$$\left.\left. + \dot{q}_o e^{-\frac{n^2\pi^2\alpha t}{l^2}}\right\}\right) \tag{B2}$$

The approximate formula used in the data reduction is

$$T_t(l,t) = \frac{\alpha}{k_{Cu} l}\frac{\dot{q}_o}{(BV_o t + 1)^3} \tag{B3}$$

The error introduced by the transient effect is thus seen to be given by all terms after the first in equation (B2).

The relative error is defined as the difference between the exact and the approximate heat-transfer rates divided by the exact heat-transfer rate. This quantity has been evaluated for V_o = 18,000 feet per second and

$B = 0.003$ second^{-1} which represent the most severe case encountered in this series of tests. The results are plotted in figure 11. The error from this source over that portion of the range where the measurements are made is seen to be less 1.5 percent.

APPENDIX C

PROPERTIES OF DISSOCIATED CARBON DIOXIDE BEHIND A SHOCK WAVE

In order to calculate theoretical heat-transfer rates, it is necessary to know the properties of the gas behind the shock wave. Study of the magnitudes of the equilibrium constants of possible chemical reactions at the high temperatures and pressures in the shock layer shows that, up to about 6000° K, the major components of a gas consisting initially of CO_2 will be CO_2, CO, O_2, and O. Thus, if the gas is treated as a mixture of ideal gases in equilibrium, the required thermodynamic properties can be calculated for various temperatures and pressures by the same procedure used to calculate the properties of high-temperature air (refs. 14 and 15). These properties can then be related to flight velocity and ambient density through the normal shock conservation equations.

The first step in this procedure is to determine the proportions of the component gases in the mixture. This is done by solving a set of four simultaneous equations in four unknowns, consisting of:

(a) One equation expressing Dalton's law of partial pressures

(b) One equation of material balance

(c) Two independent reaction equations

Dalton's law of partial pressures states that the sum of the partial pressures of the components is equal to the total pressure of the mixture. In this case, then, it follows that

$$X_{CO_2} + X_{CO} + X_{O_2} + X_O = 1 \tag{C1}$$

The material balance equation follows from the fact that in CO_2 and in any dissociation products derived from it, there will always be twice as many oxygen atoms as there are carbon atoms.

$$\frac{2X_{CO_2} + X_{CO} + 2X_{O_2} + X_O}{X_{CO_2} + X_{CO}} = 2 \tag{C2}$$

The two reaction equations are

$$CO_2 \rightleftarrows CO + \frac{1}{2} O_2 \tag{C3}$$

$$O_2 \rightleftarrows 2O \tag{C4}$$

From the law of mass action it follows that

$$\frac{(X_{CO}P)(X_{O_2}P)^{1/2}}{X_{CO_2}P} = K_{p_I} \tag{C5}$$

$$\frac{(X_{O}P)^{2}}{X_{O_2}P} = K_{p_{II}} \tag{C6}$$

where K_{p_I} and $K_{p_{II}}$ are the equilibrium constants for the indicated reactions. These constants are calculated for temperatures in the range of interest from the ideal gas free energy data of reference 9 according to the formula

$$K_p = \exp\left(-\frac{\Delta F}{RT}\right) \tag{C7}$$

When these values of K_p are inserted into equations (C5) and (C6), the equations along with equations (C1) and (C2) become the set which must be solved simultaneously for the mole fractions of the various components as a function of temperature and pressure. By substitution, these equations can be reduced to one cubic equation in one variable; if this variable is chosen to be, say, the mole fraction of O_2, then the problem is reduced to finding the real root between 0 and 1 of

$$2PX_{O_2}^{3/2} + \left(3K_{P_I} + \sqrt{K_{P_{II}}}\right)\sqrt{P}\, X_{O_2} + 2\sqrt{K_{P_{II}}}\, K_{P_I} X_{O_2}^{1/2} - K_{P_I}\sqrt{P} = 0 \tag{C8}$$

The other component mole fractions can then be found by substituting this value back into the original equations.

The next step in the procedure is to use these mole fractions to calculate the thermodynamic properties of the mixture as a function of temperature and pressure. The properties which are needed to solve the normal shock equations are the compressibility, the internal energy, and the density. Thus

$$Z_2 = \frac{m_{CO_2}}{\sum_i X_i m_i} \tag{C9}$$

$$E_2 = \sum_i Z_2 X_i E_i \tag{C10}$$

$$\rho_2 = \sum_i \frac{P_2}{Z_2 R/m_{CO_2} T_2} \tag{C11}$$

where E_i is the internal energy of the ith component of the ideal gas obtained from reference 9.

The final step in the procedure is to relate the properties on either side of the shock wave by solving the normal shock conservation equations.

The requirements of conservation of mass, momentum, and energy are, respectively,

$$\rho_1 V_1 = \rho_2 V_2 \tag{C12}$$

$$P_1 + \rho_1 V_1^2 = P_2 + \rho_2 V_2^2 \tag{C13}$$

$$E_1 + \frac{P_1}{\rho_1} + \frac{1}{2} V_1^2 = E_2 + \frac{P_2}{\rho_2} + \frac{1}{2} V_2^2 \tag{C14}$$

These equations can be combined and simplified according to the method outlined in reference 16. Then, when the properties of the ambient room-temperature CO_2 ahead of the shock are obtained from reference 9, the pressure, density, and temperature behind the shock wave can be determined for corresponding values of flight Mach number and ambient density as shown in figures 12(a), 12(b), and 12(c).

REFERENCES

1. Charters, A. C., Denardo, B. Pat, and Rossow, Vernon J.: Development of a Piston-Compressor Type Light-Gas Gun for the Launching of Free-Flight Models at High Velocity. NACA TN 4143, 1957.

2. Munk, Max M.: The Drag of Zeppelin Airships. NACA Rep. 117, 1921.

3. Hodgman, C. D., ed.: Handbook of Chemistry and Physics. 40th Edition. Chemical Rubber Pub. Co., 1958.

4. Eckert, E. R. G.: Introduction to the Transfer of Heat and Mass. 1st Edition. McGraw-Hill Book Co., Inc., 1950.

5. Fay, J. A., and Riddell, F. R.: Theory of Stagnation Point Heat Transfer in Dissociated Air. Jour. Aero. Sci., vol. 25, no. 2, Feb. 1958.

6. Eggers, A. J., Jr., Hansen, C. Frederick, and Cunningham, Bernard E.: Stagnation-Point Heat Transfer to Blunt Shapes in Hypersonic Flight, Including Effects of Yaw. NACA TN 4229, 1958.

7. Rose, P. H., and Stark, W. I.: Stagnation Point Heat-Transfer Measurements in Dissociated Air. Jour. Aero. Sci., vol. 25, no. 2, Feb. 1958. (AVCO Mfg. Corp., Res. Rep. 3, 1957.)

8. Feldman, Saul: Hypersonic Gas Dynamic Charts for Equilibrium Air. AVCO Res. Lab., 1957.

9. Hilsenrath, Joseph, et al.: Tables of Thermal Properties of Gases. National Bureau of Standards Circular 564, Nov. 1955.

10. Rutowski, R. W., and Chan, K. K.: Shock Tube Experiments Simulating Entry into Planetary Atmospheres. American Astronautical Society, Preprint 59-26, 1959.

11. Thomas, M.: The High Temperature Transport Properties of Carbon Dioxide. Rep. SM-37790, Douglas Aircraft Co., July 1960.

12. Terman, F. E.: Radio Engineering. 2nd Edition. McGraw-Hill Book Co., Inc., 1937.

13. Churchill, R. V.: Modern Operational Mathematics in Engineering. 1st Edition. McGraw-Hill Book Co., Inc., 1944.

14. Krieger, F. J., and White, W. B.: The Composition and Thermodynamic Properties of Air at Temperatures from 500 to 8000° K and Pressures from 0.00001 to 100 Atmospheres. Rand Rep. R-149, 1949.

15. Gilmore, F. R.: Equilibrium Composition and Thermodynamic Properties of Air to 24000° K. Rand Rep. RM 1543, 1955.

16. Hochstim, A. R.: Gas Properties Behind Shocks at Hypersonic Velocities. I. Normal Shocks in Air. Convair Report ZPh(GP)-022, Jan. 1957.

Page intentionally left blank

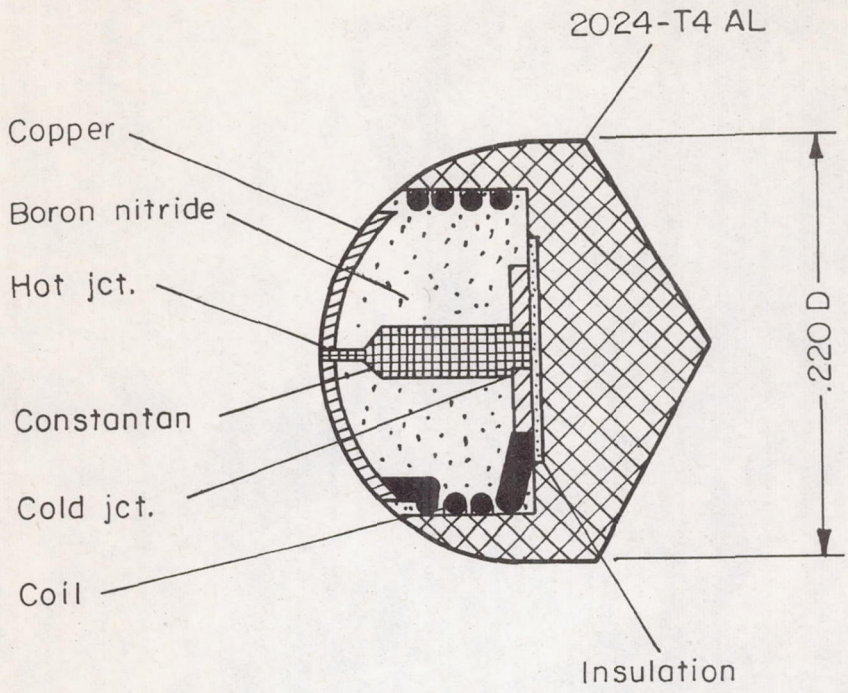

Model wt. approx. 0.18g
Nose radius .110 in.
Nose thickness .0075 in.

Figure 1.- Model.

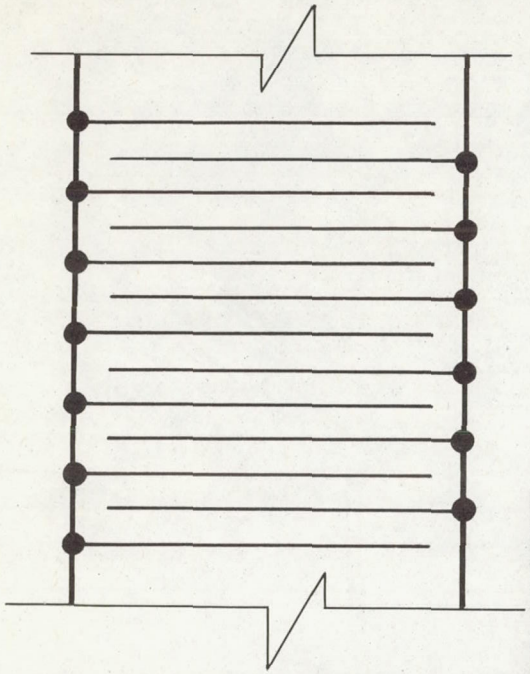

Detail: SHIELDING
IN COIL FORM
(UNROLLED)

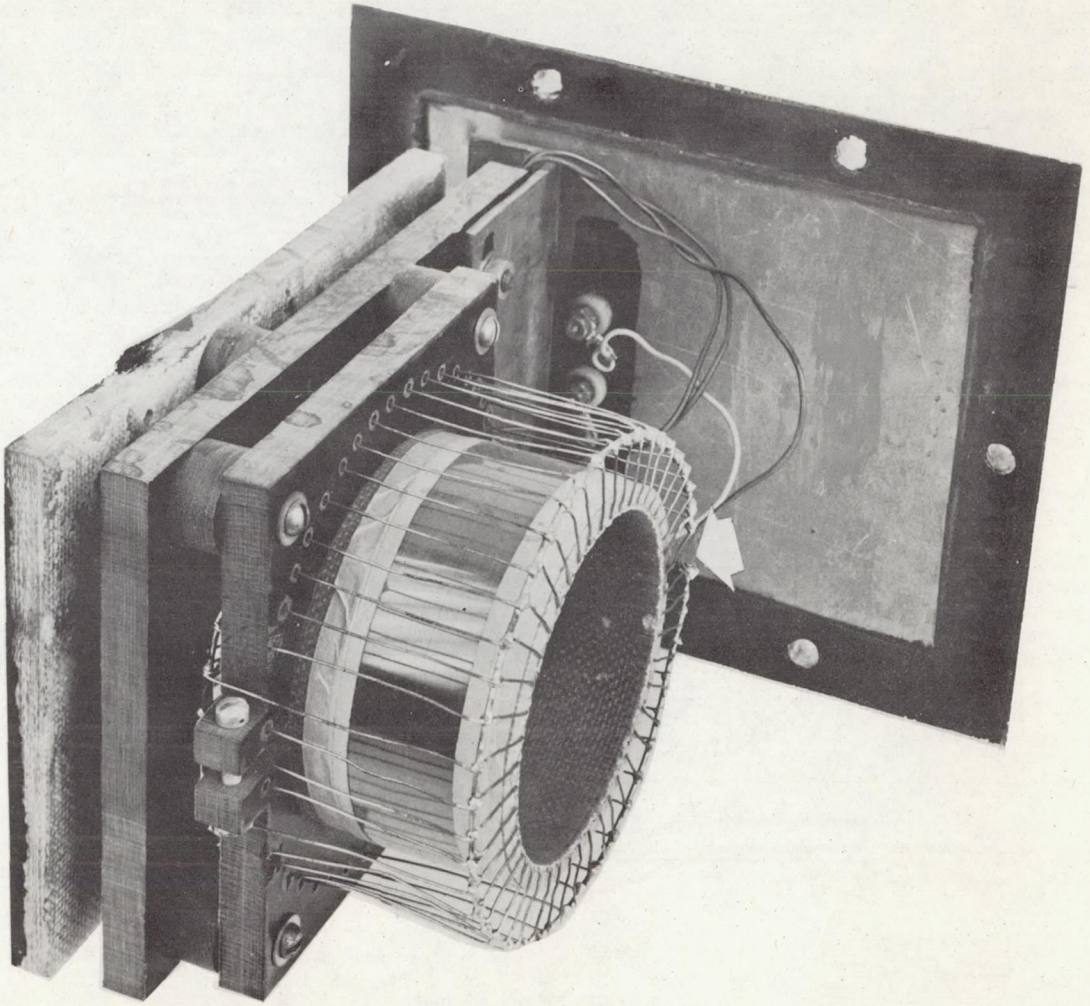

Figure 2.- Pickup coil.

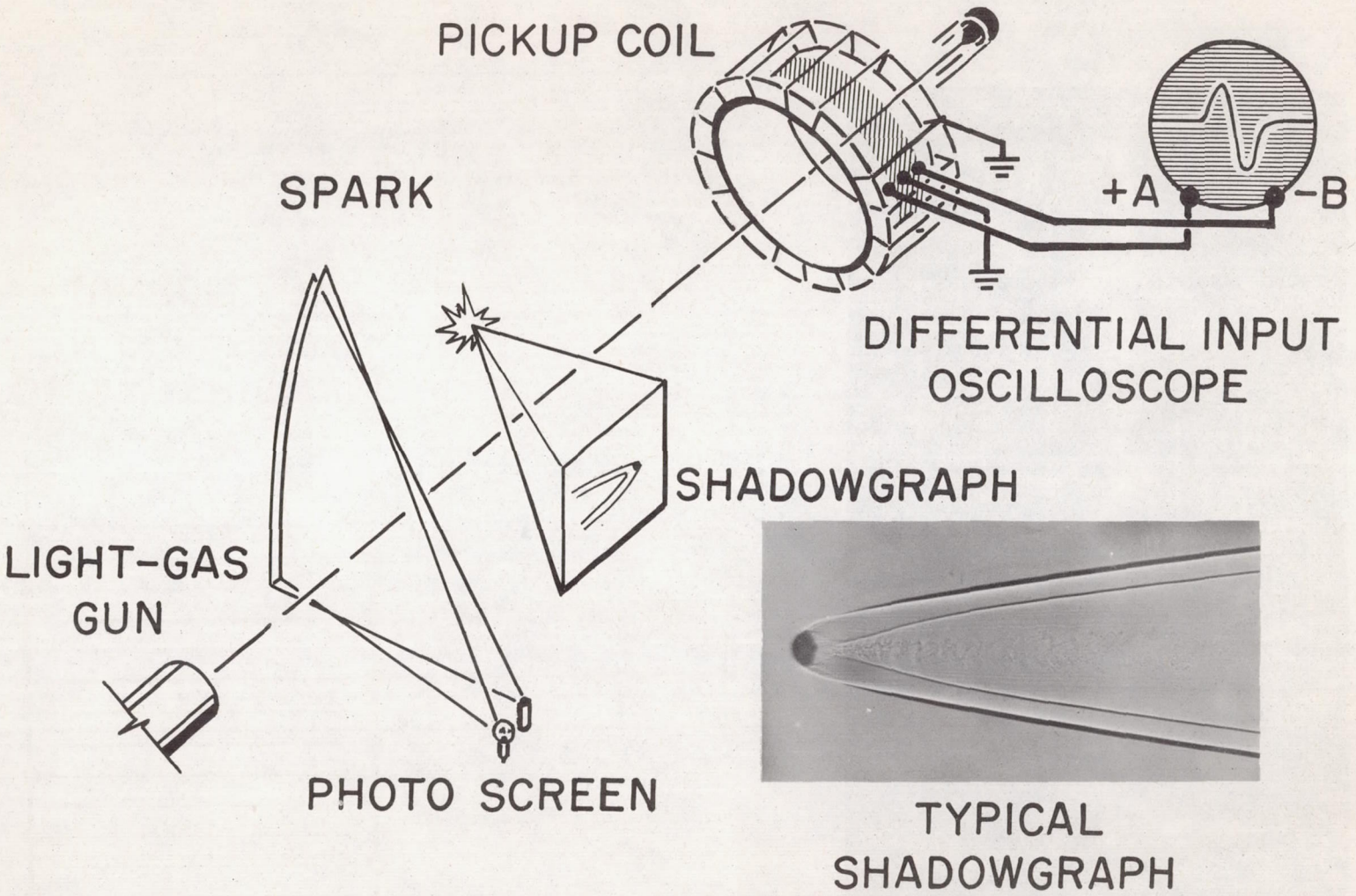

Figure 3.- Experimental setup.

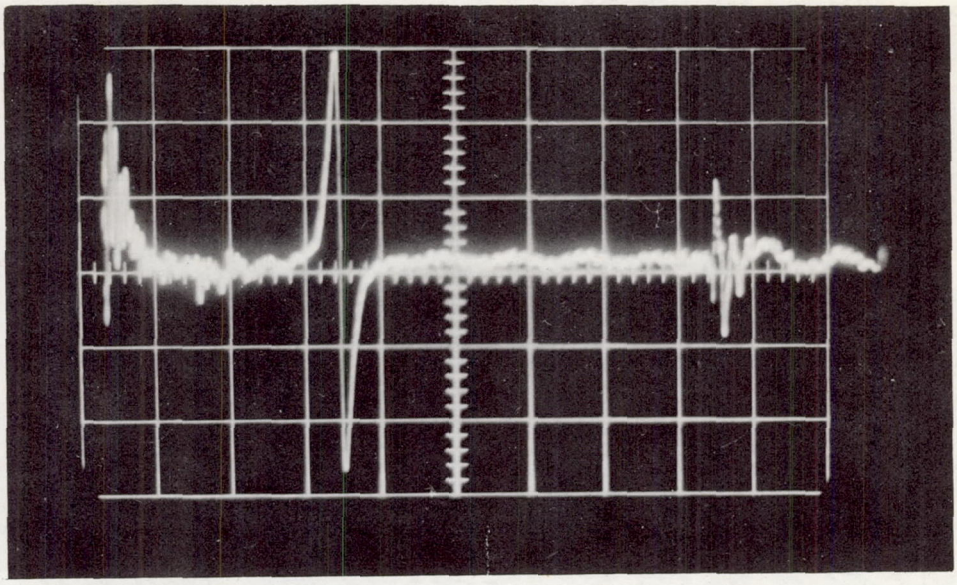

Amplitude 1 mv/div
Sweep rate 100μsec/div
Launch velocity 11,000 ft/sec
1/10 atm. CO_2

Figure 4.- Typical oscilloscope record.

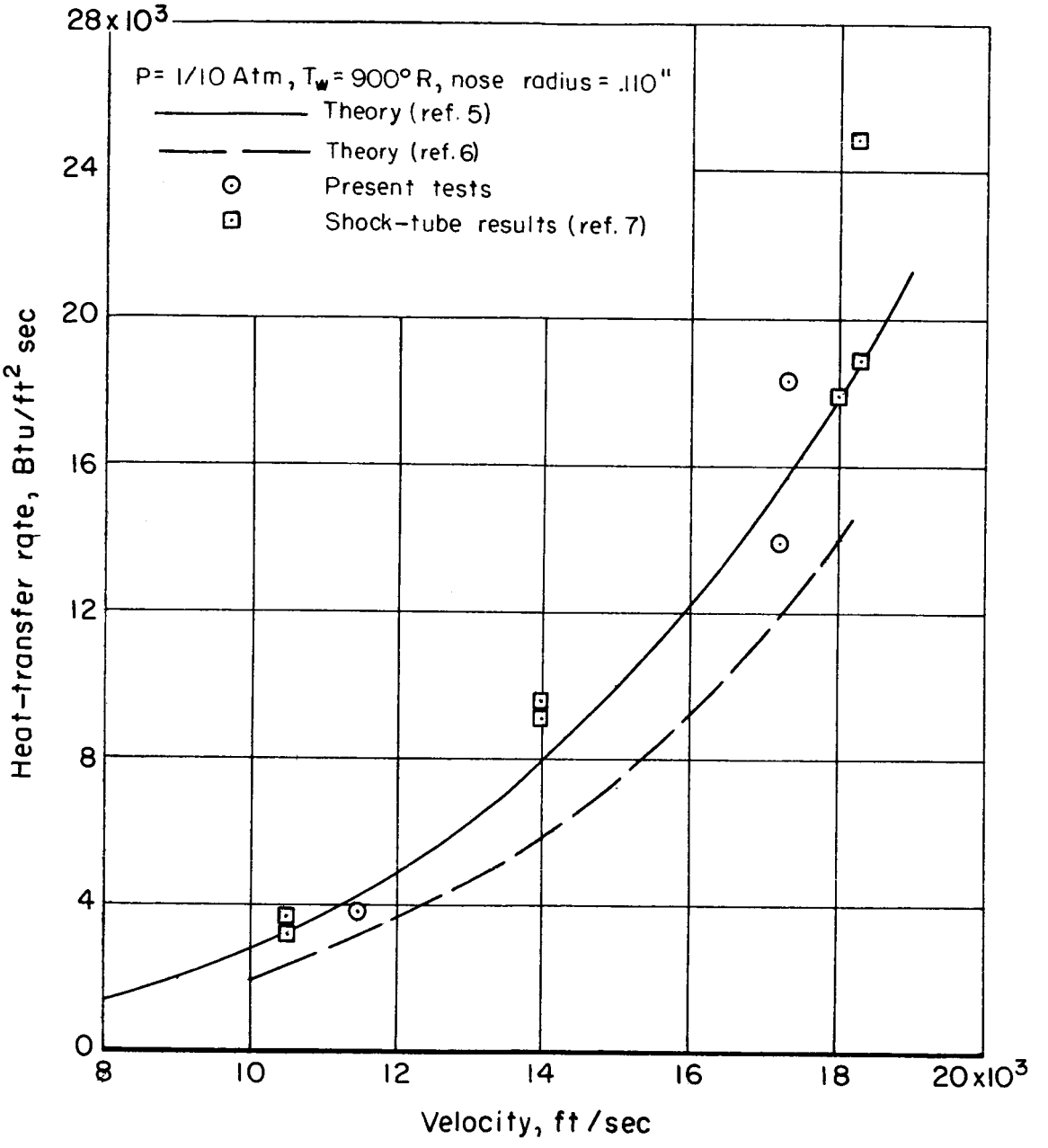

Figure 5.- Stagnation-point heat-transfer rate in air.

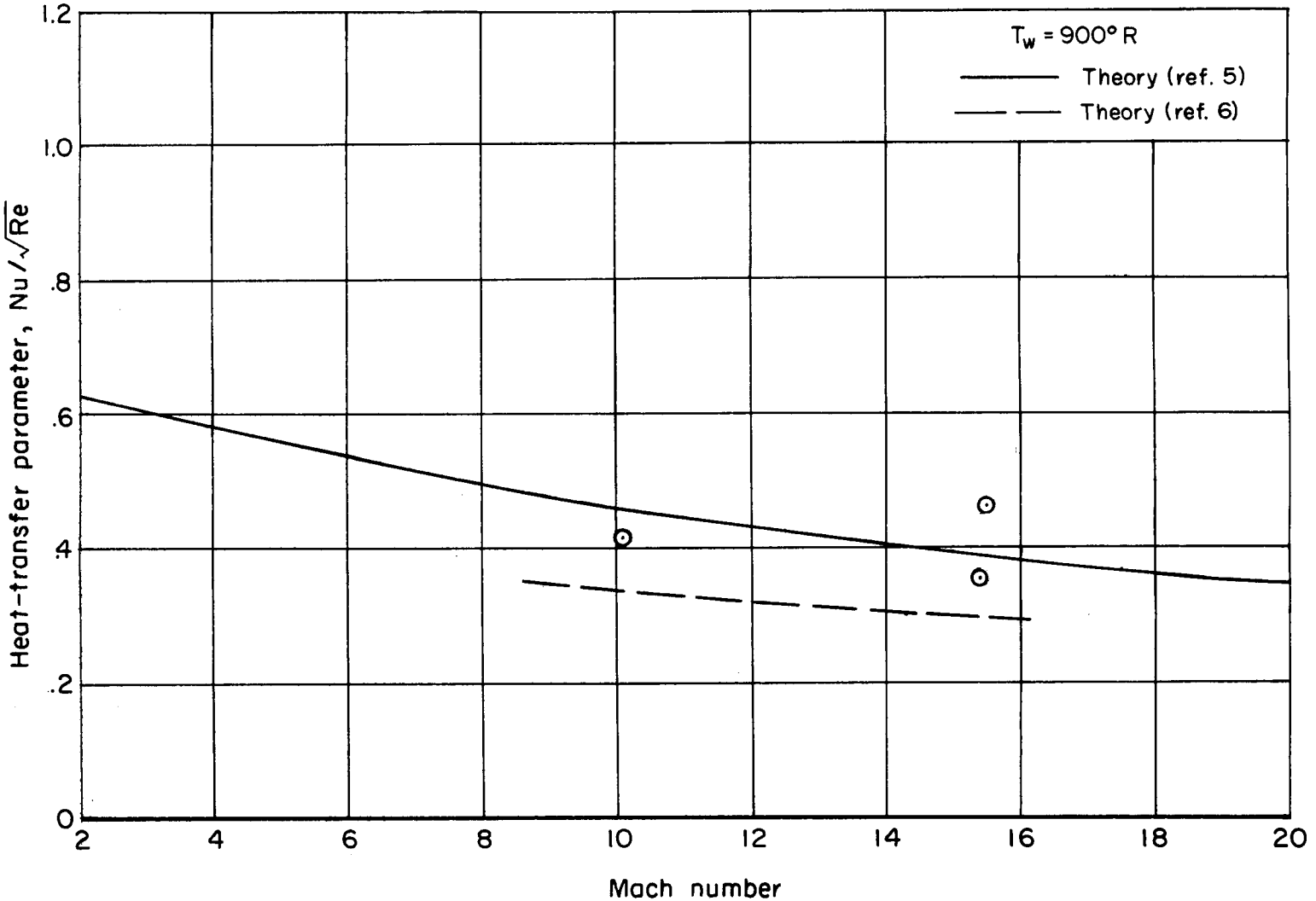

Figure 6.- Stagnation-point heat transfer in air.

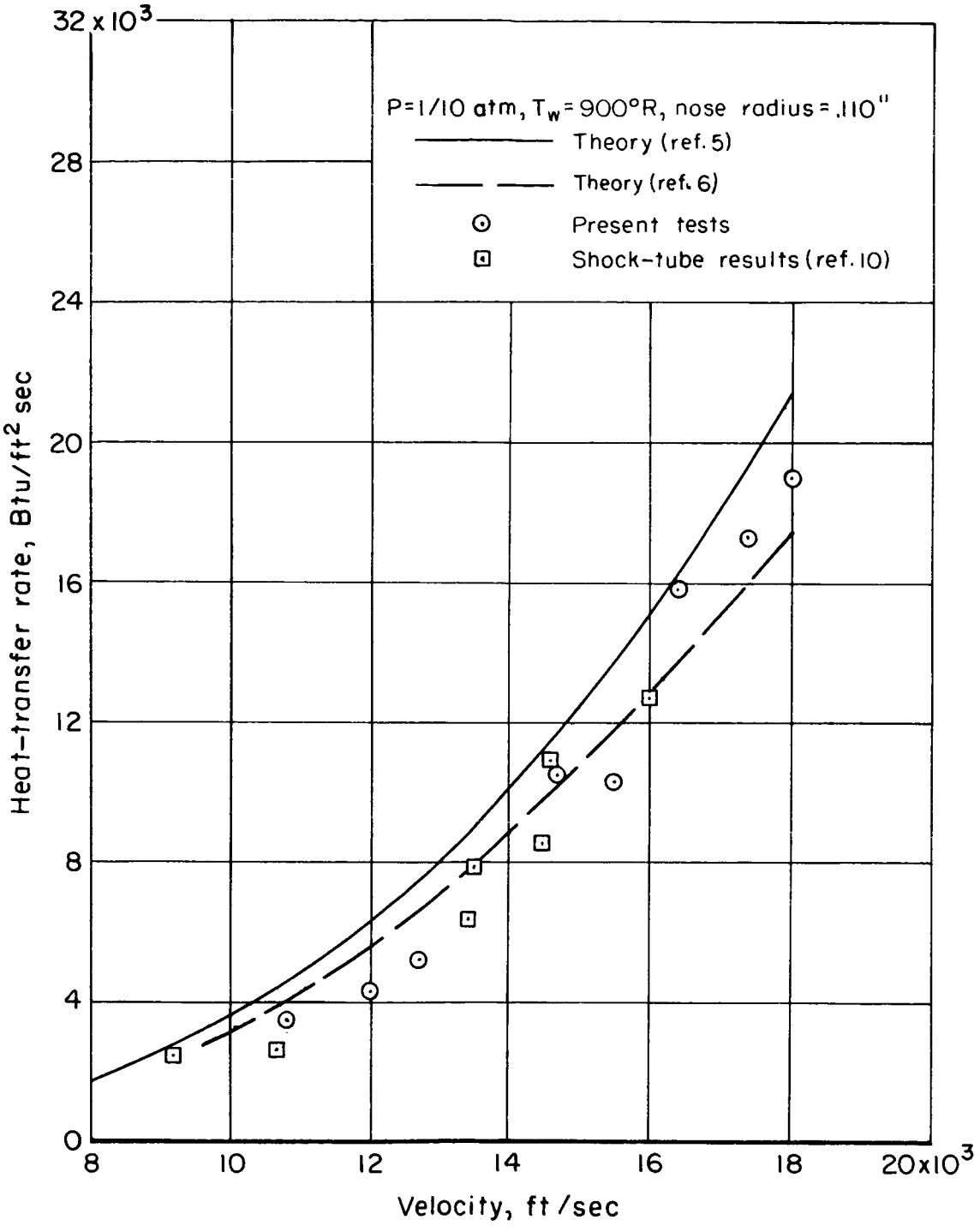

Figure 7.- Stagnation-point heat-transfer rate in carbon dioxide.

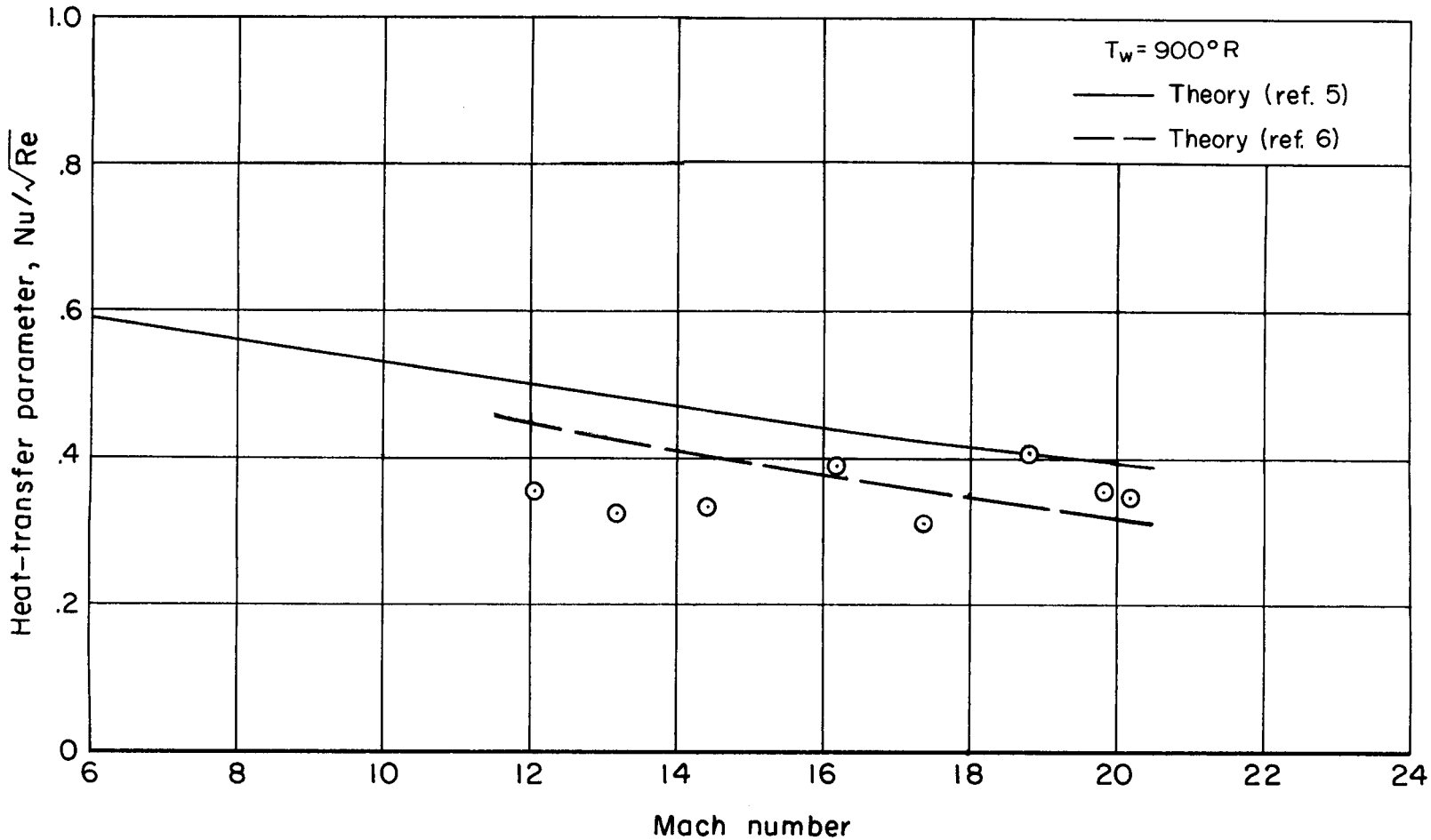

Figure 8.- Stagnation-point heat transfer in carbon dioxide.

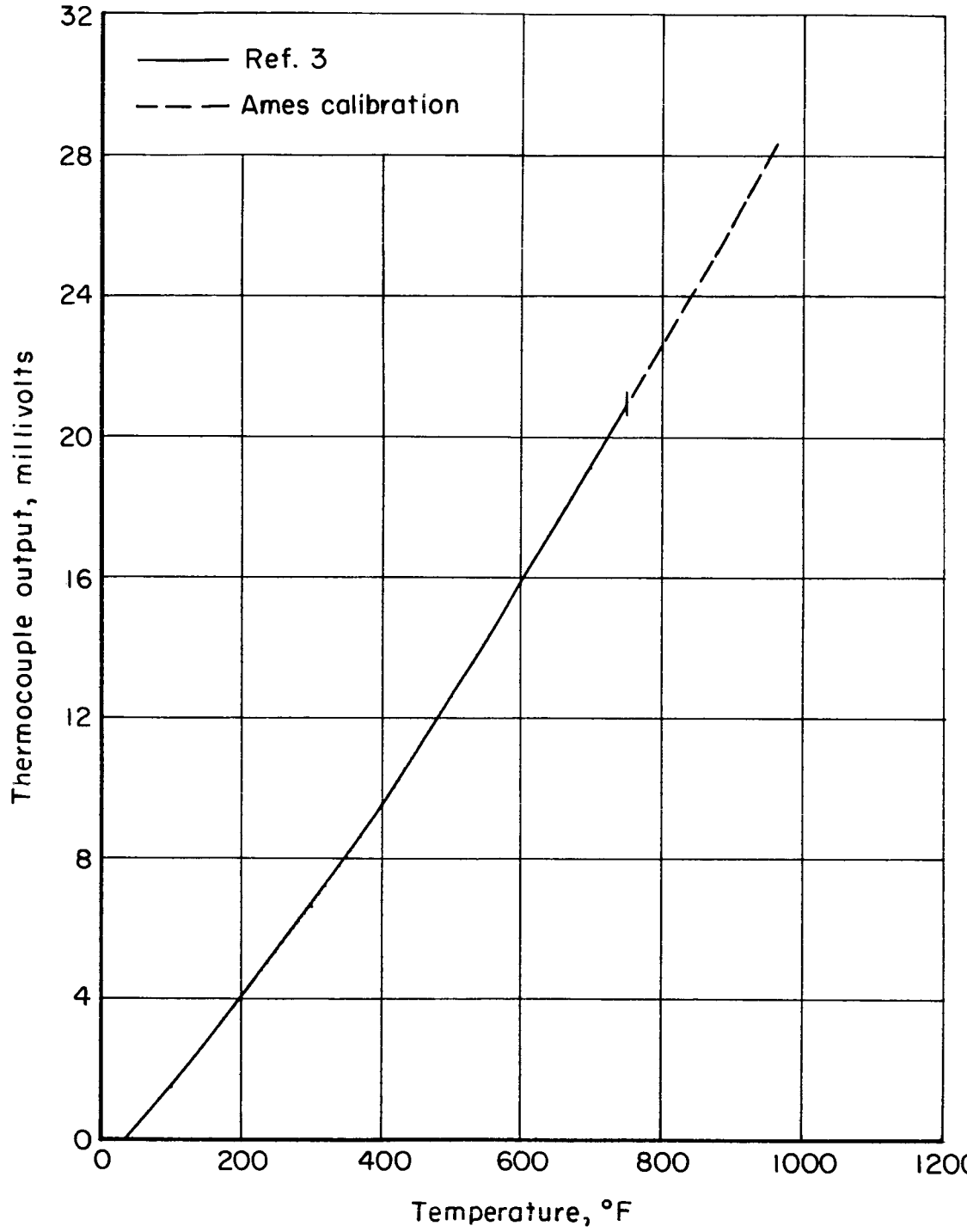

Figure 9.- Copper-constantan thermocouple calibration.

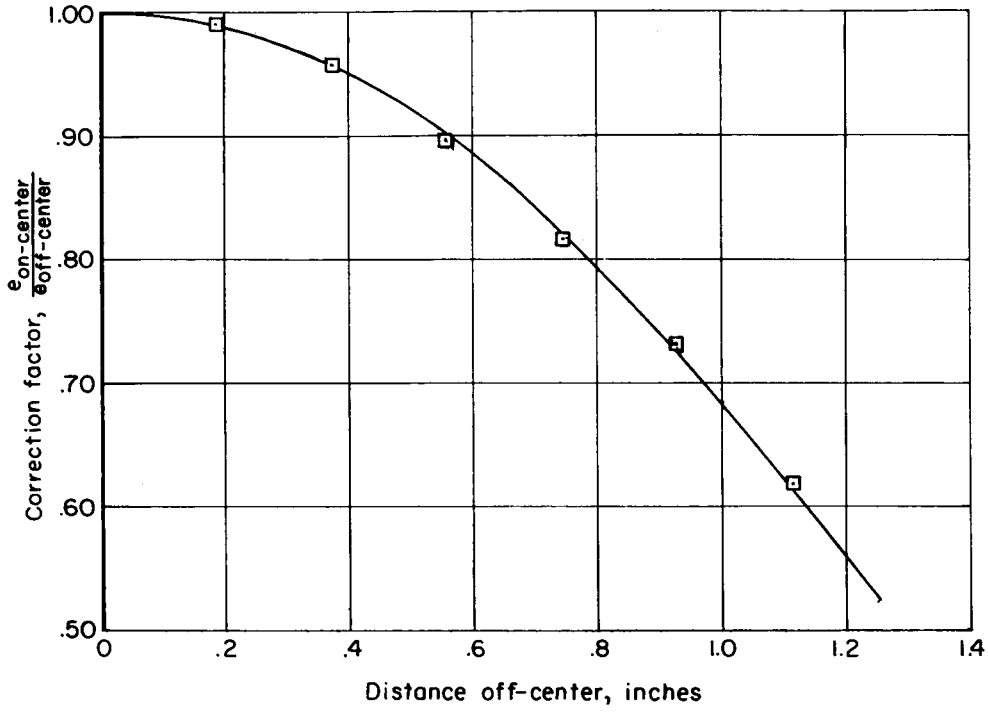

Figure 10.- Correction factor for off-center shot.

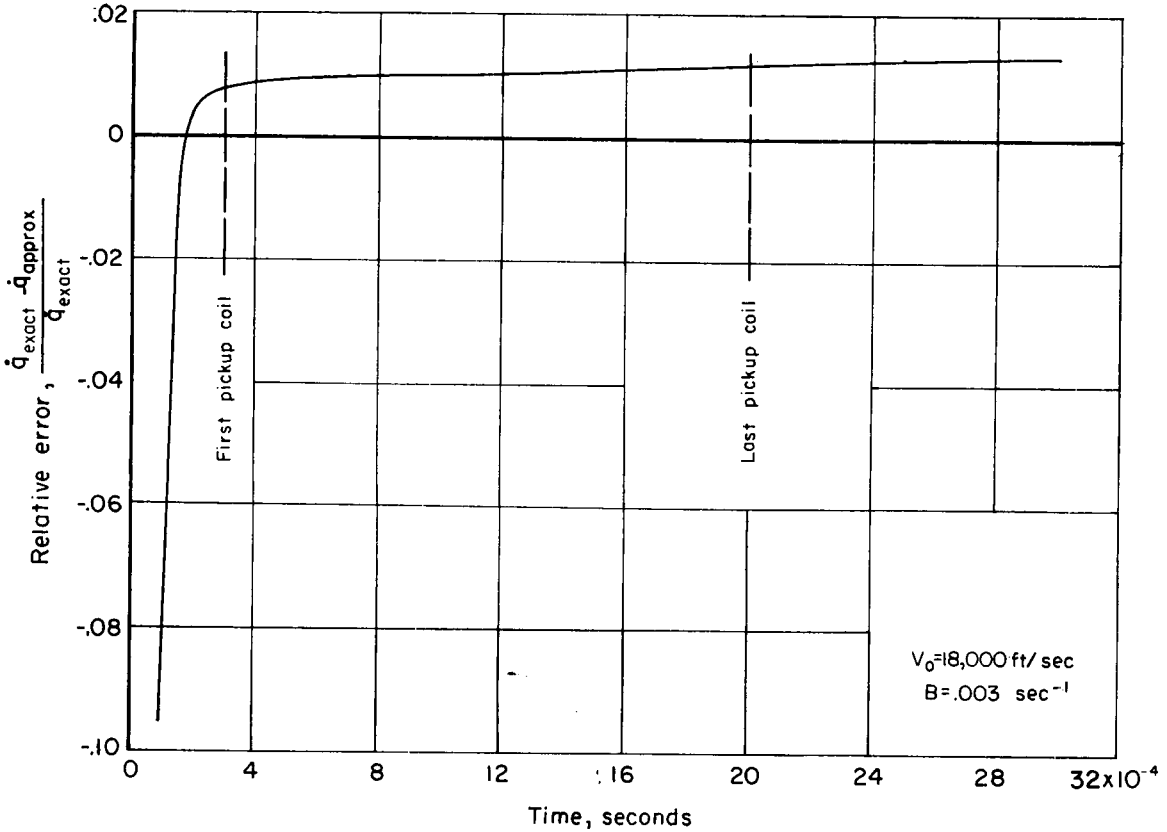

Figure 11.- Relative error in heat-transfer rate due to transients.

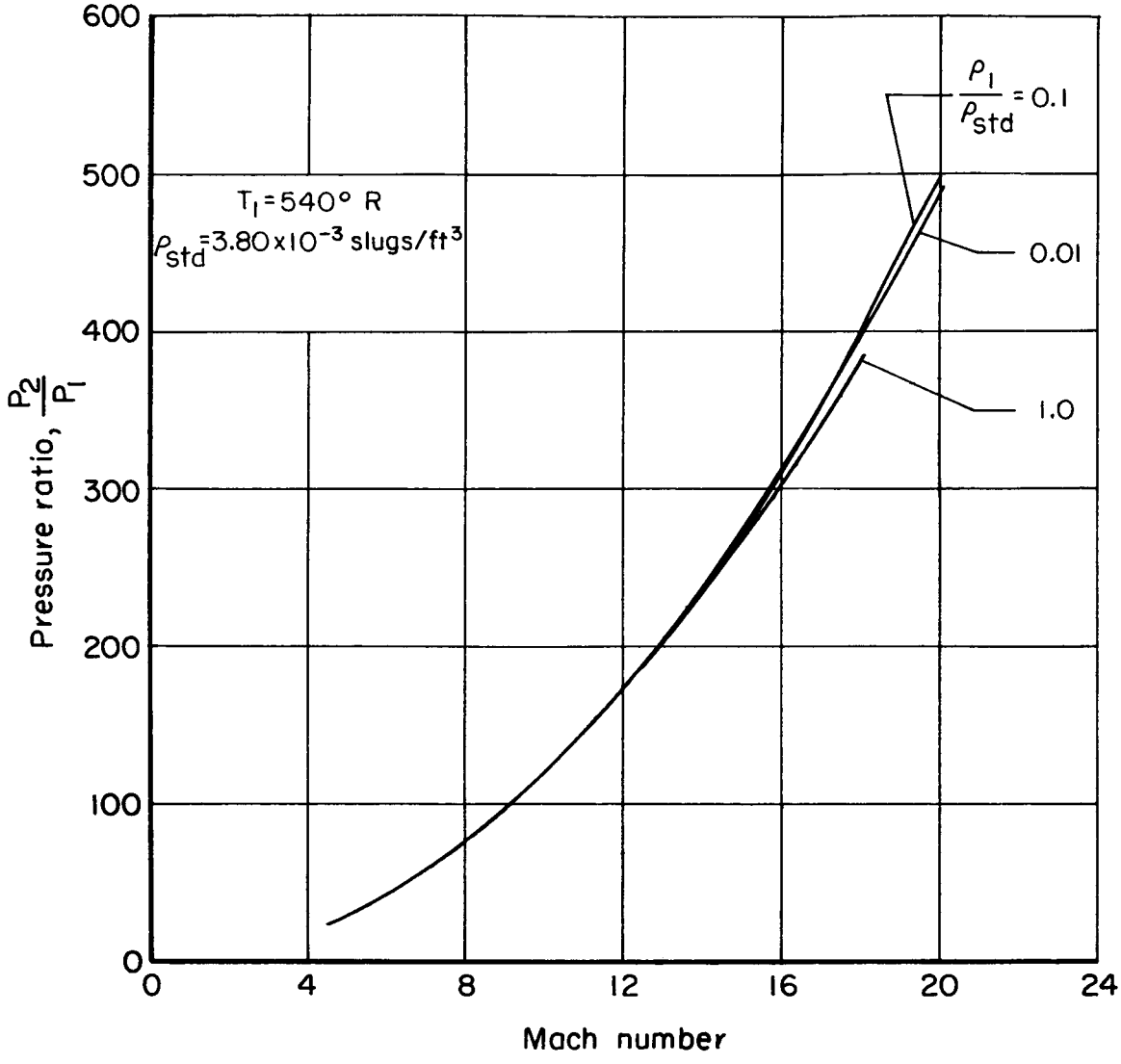

(a) Pressure ratio.

Figure 12.- Ratios of pressure, density, and temperature across a normal shock wave in carbon dioxide.

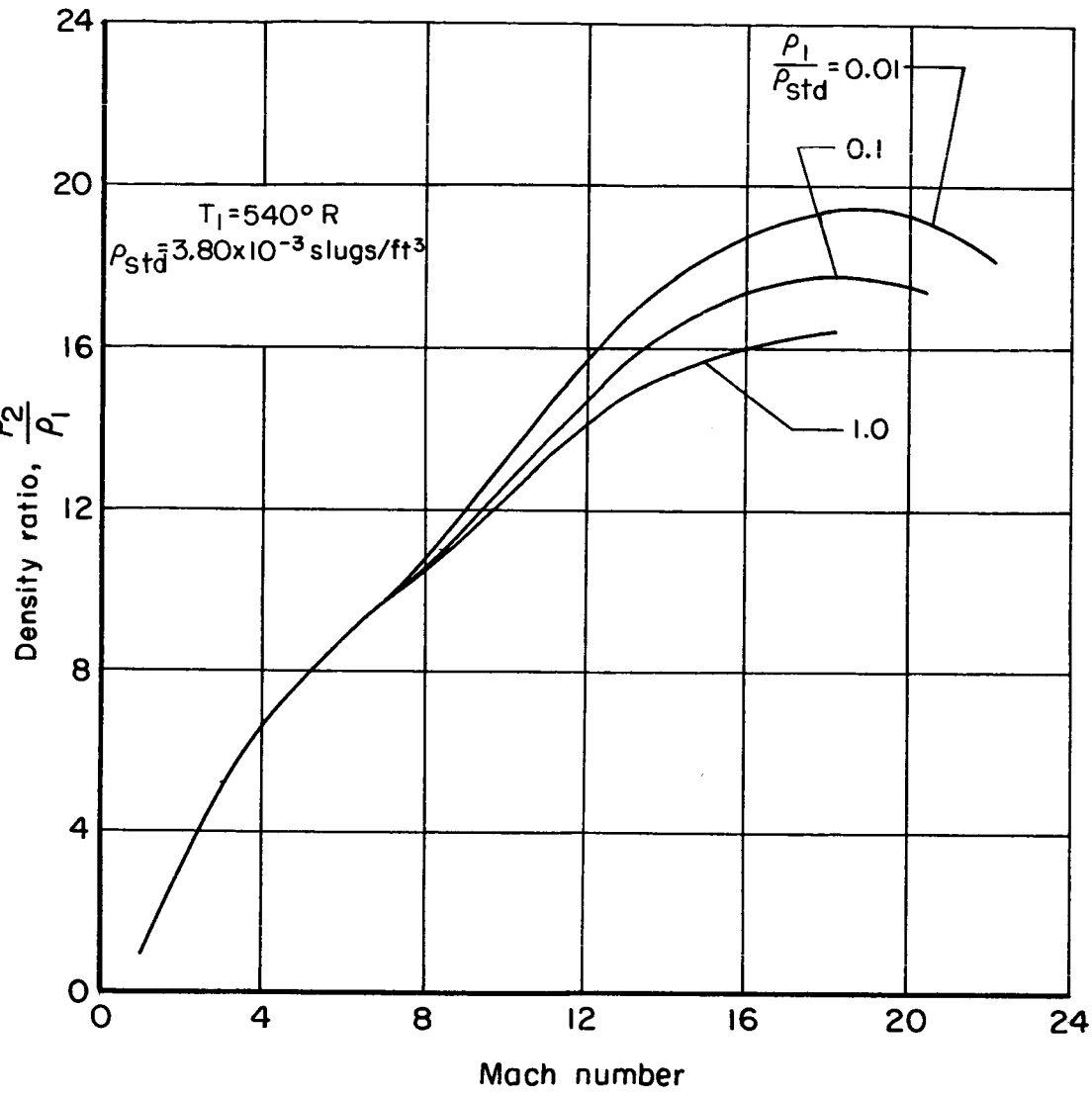

(b) Density ratio.

Figure 12.- Continued.

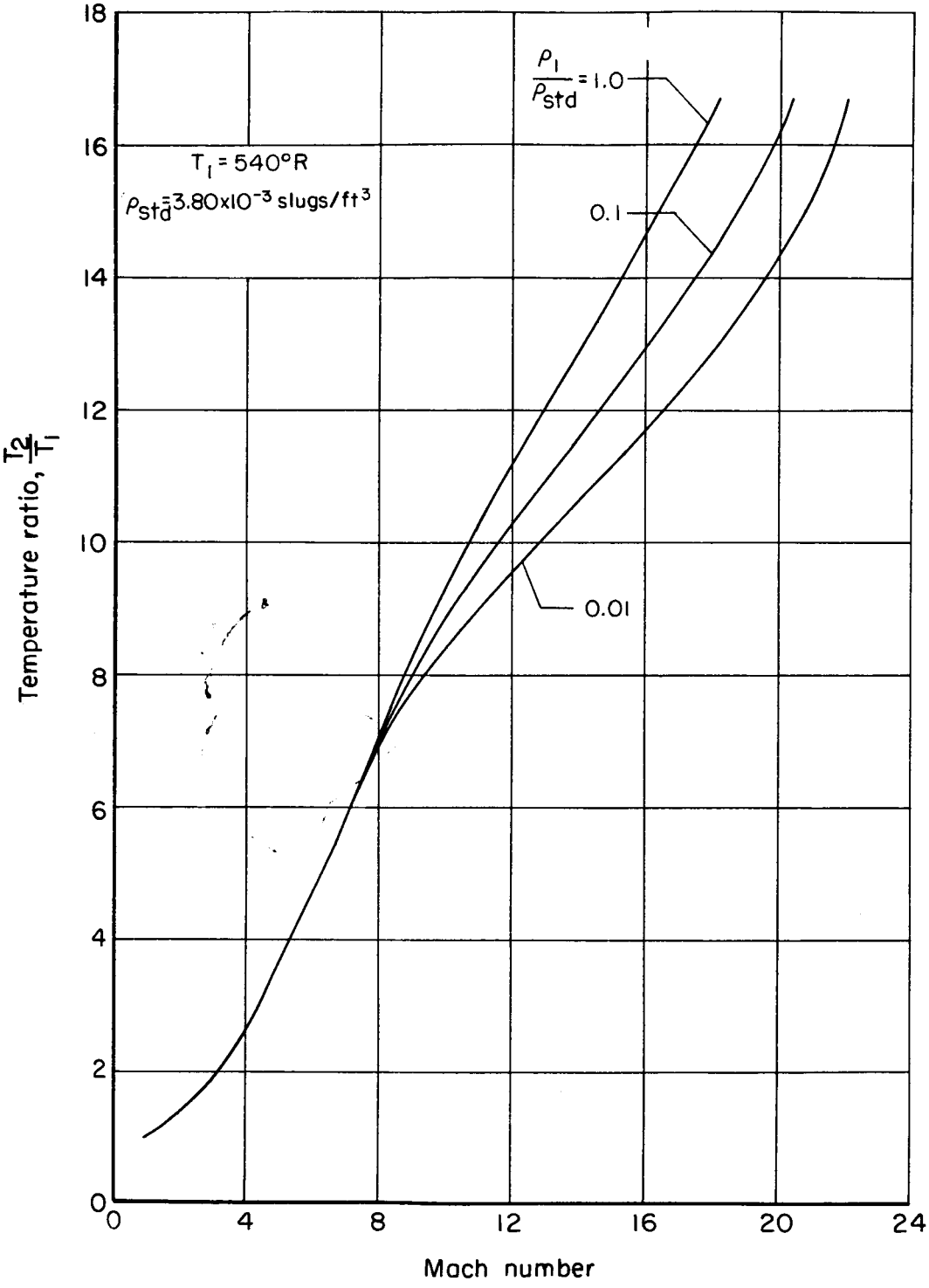

(c) Temperature ratio.

Figure 12.- Concluded.